Atmospheric Environment 179 (2018) 107–117

Contents lists available at ScienceDirect

Atmospheric Environment

journal homepage: www.elsevier.com/locate/atmosenv

Estimation of atmospheric columnar organic matter (OM) mass concentration from remote sensing measurements of aerosol spectral refractive indices

Ying Zhang[a], Zhengqiang Li[a,*], Yele Sun[b], Yang Lv[a], Yisong Xie[a]

[a] State Environmental Protection Key Laboratory of Satellite Remote Sensing, Institute of Remote Sensing and Digital Earth, Chinese Academy of Sciences, Beijing 100101, China

[b] Institute of Atmospheric Physics, Chinese Academy of Sciences, Beijing 100029, China

ARTICLE INFO

Keywords:
Organic matter
Chemical components
Remote sensing
Aerosol
Hygroscopicity

ABSTRACT

Aerosols have adverse effects on human health and air quality, changing Earth's energy balance and lead to climate change. The components of aerosol are important because of the different spectral characteristics. Based on the low hygroscopic and high scattering properties of organic matter (OM) in fine modal atmospheric aerosols, we develop an inversion algorithm using remote sensing to obtain aerosol components including black carbon (BC), organic matter (OM), ammonium nitrate-like (AN), dust-like (DU) components and aerosol water content (AW). In the algorithm, the microphysical characteristics (i.e. volume distribution and complex refractive index) of particulates are preliminarily separated to fine and coarse modes, and then aerosol components are retrieved using bimodal parameters. We execute the algorithm using remote sensing measurements of sun-sky radiometer at AERONET site (Beijing RADI) in a period from October of 2014 to January of 2015. The results show a reasonable distribution of aerosol components and a good fit for spectral feature calculations. The mean OM mass concentration in atmospheric column is account for 14.93% of the total and 56.34% of dry and fine-mode aerosol, being a fairly good correlation (R = 0.56) with the in situ observations near the surface layer.

1. Introduction

Aerosol, pending particulate matter in the atmosphere, can not only influence human health causing air pollution, but also reduce the solar radiation and energy budget leading to climate changes (Boucher et al., 2013). Because the different aerosol component may present different spectral characteristics, the aerosol components can be retrieved using optical remote sensing technology. Based on this principle, Satheesh et al. (1999, 2002); Satheesh and Srinivasan (2002); Satheesh and Krishna (2005) developed a remote sensing inversion algorithm of aerosol components which assumed aerosols to be external mixed. However, the method using the fixed size distribution of each aerosol component, which should vary in the real atmosphere. The internal mixing hypotheses are also widely used because its merit on the weak dependence of size distribution and relatively accurate calculation of the aerosol scattering and absorbing characteristics (Schuster et al., 2005, 2009, 2015; Arola et al., 2011; Li et al., 2013; Wang et al., 2013). For absorbing component (e.g. black carbon) coexisting with non-absorbing components (e.g. water content, sulfate, nitrate and ammonium) in aerosols, the absorbing component can be separated from the spectral differences based on remote sensing measurements (Schuster et al., 2005). Schuster et al. (2009) also estimated the dust component which is typically coarse modal particles and with relatively weak light absorbing characteristic (Yang et al., 2009). Similarly, Arola et al. (2011) estimated the brown carbon which presents the optical absorbing characteristic mainly from 200 to 550 nm (Andreae and Gelencsér, 2006), but assuming the conditions with ignoring dust component. In order to distinguish spectrally absorbing components (e.g. brown carbon and dust), the slope of SSA spectrum between 440 and 675 nm is introduced into retrieval processing (Wang et al., 2013). Li et al. (2013) separate several optical absorbing components (i.e. BC, brown carbon and dust) from the optical scattering components using internal mixing hypotheses. They extended the species of remotely sensed aerosol components to five kinds. Moreover, aerosol bimodal characteristics are used to estimate the aerosol absorbing components including BC, brown carbon and hematite in fine and coarse mode (Schuster et al., 2015). However, most researches focus on the estimated aerosol components and fail to develop the new species retrieval (e.g. Li et al., 2015; Zhang et al., 2015; Xie et al., 2014).

Recently, many studies find that organic matter (OM), composed of

* Corresponding author.
E-mail address: lizq@radi.ac.cn (Z. Li).

https://doi.org/10.1016/j.atmosenv.2018.02.010
Received 10 May 2017; Received in revised form 31 January 2018; Accepted 4 February 2018
Available online 10 February 2018
1352-2310/ © 2018 Elsevier Ltd. All rights reserved.

water-insoluble (WIOM) and water-soluble organic matter (WSOM), played a important role and accounts for about 20–50% in aerosols (Sun et al., 2016; Chan and Yao, 2008; Cao et al., 2007, 2004, 2003; Putaud et al., 2004; Saxena and Hildemann, 1996). But only a few studies separated the OM based on remote sensing measurements (Xie et al., 2017; Choi and Ghim, 2016). Xie et al. (2017) added the sea salt and particulate organic matter based on the method of Li et al. (2013) to extend the species to seven kinds, but the weak hygroscopic characteristics of organic matter are not included in the algorithm. Similarly, the water-soluble and insoluble organic carbons in fine mode are considered in the research of Choi and Ghim (2016), but the water-soluble organic carbon is hard to distinguish from inorganic salts without regard to aerosol hygroscopic growth.

In this study, we separate the OM (including WIOM and WSOM) from aerosol using the strong scattering and weak hygroscopic characteristics of OM (Li et al., 2014a,b), and improve the classification of aerosol species in condition of volume balance. This study fill up the gap of measurement mode between chemical analysis and remote sensing and decrease the estimated component biases. The methodology of inversion algorithm described in section 2. Section 3 shows the results and comparisons with chemical analysis, and conclusions and discussions are listed in section 4.

2. Methodology

2.1. Hygroscopicity characteristics of OM components

In order to retrieve the OM component, we separate the aerosol size distribution into fine and coarse mode in advance. Due to the anthropogenic OM mainly from fine mode, the algorithm in this study is not involved the OM component in coarse mode (e.g. fungus, spore). Therefore, in coarse mode there are only two components including dust-like (DU) and aerosol water content (AW_c), while five components in fine mode (i.e. BC, WSOM, WIOM, ammonium nitrate-like (AN) and AW_f) is a challenge in this study.

For estimating the aerosol components in the fine mode, hygroscopic difference between OM and AN component as an extra constrained condition is applied to the algorithm coupled with the condition of light-absorbing difference. Fig. 1 shows the geometric growth factors (GF) of typical inorganic salts and OMs (including WIOM and WSOM) in laboratory, and the GFs of these components present a significant difference (Sjogren et al., 2007; Prenni et al., 2003). GFs of inorganic salts are all larger than 1.5 (Hu et al., 2010), while that of OMs are much smaller than inorganic salt with mean value of 1.1 (Varutbangkul et al., 2006) except the low content of malonic acid and levoglucosan components in the aerosols (Jing et al., 2016; Liu et al., 2016). Therefore, the OM regards as the low hygroscopic components can be distinguished with AN. However, the OM mixture includes WSOM and WIOM, which can be only distinguished by the phase state and slight difference in imaginary part of atmospheric aerosol complex refractive index (CRI). Thus, the empirical relationship of the ratio of WSOM in the total OM is used to constrain the iteration process for the fine mode, which is descripted in section 2.3.1.

2.2. The aerosol composition model and component separation

The algorithm consists of two parts, including the estimation of atmospheric aerosol CRI (Zhang et al., 2017), denoted by $m = n - ik$, and components (this study). For the first part, the aerosol CRIs are separated into fine and coarse mode and iterated through fitting measurements with the inputs of aerosol optical depth (τ), absorbing aerosol optical depth (τ_a) and volume particle size distribution (VPSD). τ at five wavelengths (440, 500, 675, 870, 1020 nm) and τ_a at four (440, 675, 870, 1020 nm) are used in the retrieval process, and then fine- and coarse-mode CRIs at four wavelengths can be obtained and is applied to the aerosol component retrievals. In this study, the aerosol CRIs and

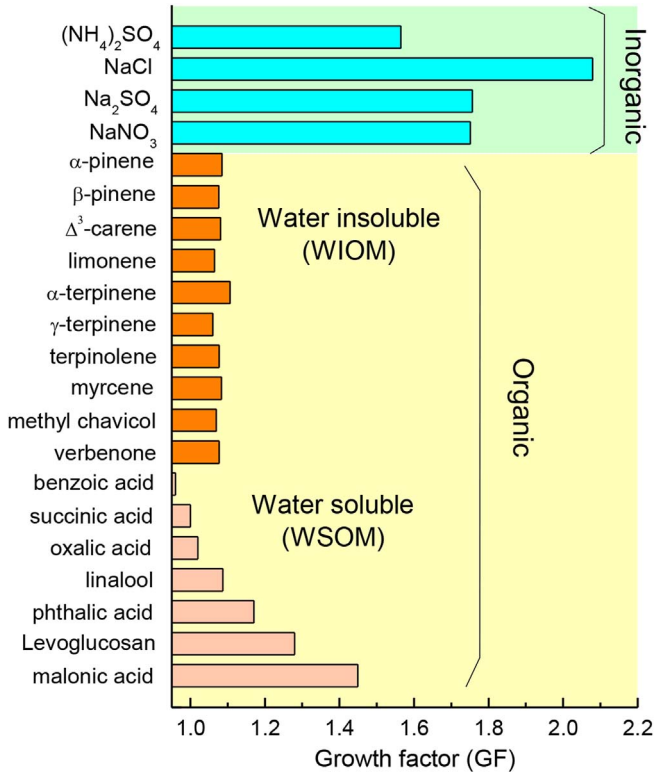

Fig. 1. Different geometric hygroscopic growth factor between inorganic and organic aerosols with RH around 85% of relative humidity. (Jing et al., 2016; Liu et al., 2016; Shi et al., 2012; Hu et al., 2010; Varutbangkul et al., 2006).

VPSD in fine and coarse mode (Zhang et al., 2016, 2017) are used as the input data for the aerosol components retrieved by remote sensing measurements. The CRI inputs include the real and imaginary parts in fine mode at four wavelengths as well as τ_a and only the imaginary part in coarse mode at 675 nm due to the low retrieved accuracy in coarse mode (Zhang et al., 2017).

For the second part, the species classification of aerosol components shows in Fig. 2 and the steps of inversion algorithm as follows: (1) estimation of CRIs for the fine and coarse modes; (2) the separation between water-soluble and water-insoluble matters; (3) estimates proportion of AN and AW_f depended on hygroscopic growth factor; (4) the separation between WSOM and AN depended on hygroscopic difference; (5) the separation between WIOM and BC depended on spectral difference; (6) estimates aerosol water content in coarse mode.

We classified the aerosol into five main species (BC, OM, AN, AW, DU) as illustrated in Fig. 2. In the five main species, OM and DU are the mixtures and thus the CRIs are determined like below. For OM, real part (n) at all wavelengths are according to Sun et al. (2007) and imaginary part (k) are according to Chen and Bond (2010). For DU, 5% (amount to 2.24% in volume percent) of hematite as light-absorbing dust and 95% of illite as light-scattering dust are mixed to calculate the CRIs of DU (Schuster et al., 2015; Lafon et al., 2004; Wagner et al., 2012). Other CRIs of BC, AN and AW and the effective densities are listed in Table 1.

2.2.1. Estimation of CRIs for the fine and coarse modes

In order to separate CRIs for different modes, we need to separate the VPSD into complete log-normal functions firstly following the VPSD breakdown method described in Cuesta et al. (2008). The multi-modal log-normal distributions fits the AERONET-retrieved VPSD by the following formula:

$$\frac{dV(r)}{dlnr} = \sum_{i=1,m} \frac{C_i}{\sqrt{2\pi}\,|ln\sigma_i|} exp\left[-\frac{1}{2}\left(\frac{lnr - lnr_i}{ln\sigma_i}\right)^2\right],\ \text{m= 1,2,\&...,} \quad (1)$$

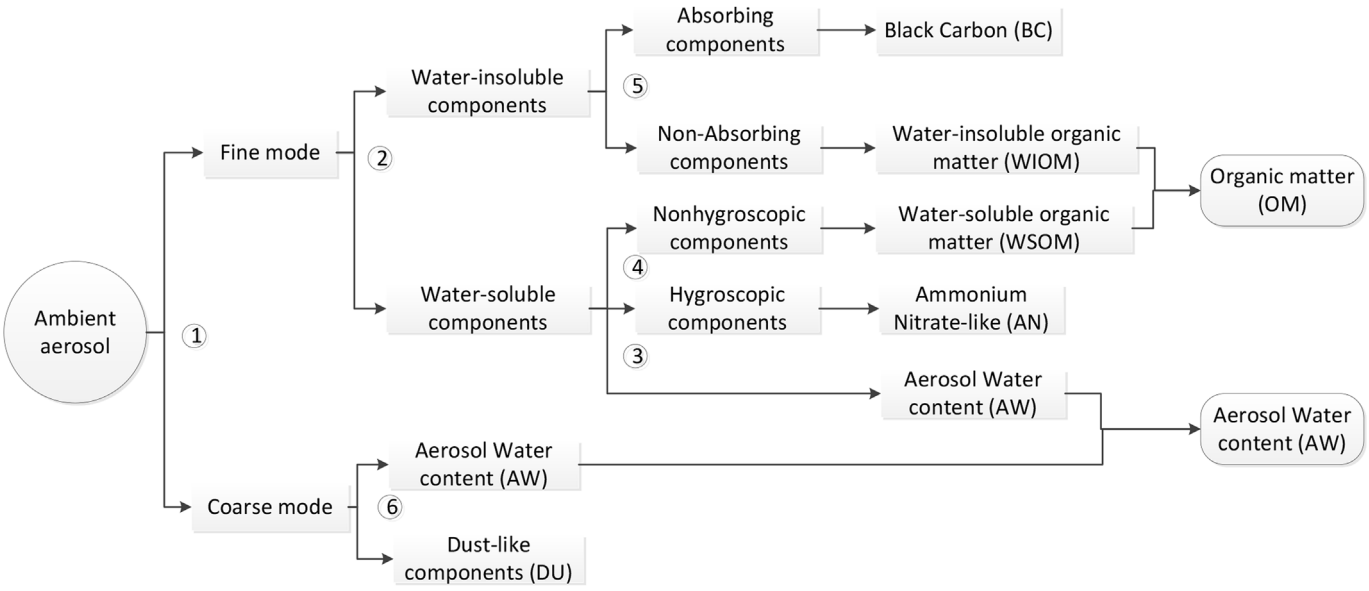

Fig. 2. Flowchart of the aerosol component classification in inversion algorithm.

where $dV/d\ln r$ (in unit of $\mu m^3/\mu m^2$) is the volume particle size distribution, C_i ($\mu m^3/\mu m^2$), r_i (μm), and ln σ_i are the volume modal concentration, median radius, and standard deviation of ln r_i for each LNM mode, respectively. Based on the separated VPSD for the fine and coarse mode, a limited-memory optimization algorithm is employed to retrieve the CRIs. The real part (n) of sub-CRIs is spectrally independent, and the imaginary part (k) of sub-CRIs has spectral variation as follows:

$$n_{f/c}(\lambda) = n_{f/c}$$
$$k_{f/c}(\lambda) = \begin{cases} k_{f/c,440} \\ k_{f/c} \end{cases} \quad (2)$$

where λ denotes standard wavelength of AERONET products and "*f*" and "*c*" represent the fine and coarse modes, respectively. The details of separated CRIs method can be found in Zhang et al. (2017).

2.2.2. The separation between water-soluble and water-insoluble matters

The ratio of water-soluble (e.g. WSOM and AN) to water-insoluble (e.g. BC and WIOM) volume fraction of atmospheric aerosol is proposed and parameterized with real part of CRI, aerosol diameter and type estimation in the study of Schuster et al. (2009). However, the relatively high real part of CRI in condition of high RH level can inhibit the water-soluble volume fraction and underestimate the water-soluble components because of no regard for WSOM component in the Schuster's algorithm (2009). Therefore, we replace the real part of CRI with RH to re-parameterize as follows:

$$\begin{cases} f_i/f_s = \psi(RH)\int \varepsilon(D)dD \\ \psi(RH) = 5.74(1 - RH)^3 + 0.01 \end{cases} \quad (3)$$

where, f_i and f_s are the water-insoluble and water-soluble volume fraction, respectively. $\psi(RH)$ is the re-parameterized function with *RH*. *RH* is the air relative humidity and *D* is the aerosol diameter. $\varepsilon(D)$ is a ratio of water-soluble to water-insoluble volume fraction of atmospheric aerosol in climatology (Kandler and Schütz, 2007). It can be expressed as

$$\varepsilon(D) = \varepsilon_0 + \varepsilon_v \cdot exp\left[-\left(\frac{\log(D/d_0)}{\sigma_{log}}\right)^2\right] \quad 0.01\ \mu m < D < 16\mu m \quad (4)$$

where, ε_0, ε_v, d_0, σ_{log} are the fitting parameters averaged in four aerosol types (i.e. maritime, urban, continental and free tropospheric), which can represent the aerosol property in general conditions (values listed in Table 1 in Kandler and Schütz, 2007).

2.2.3. Estimate of proportion of AN and AW_f depended on hygroscopic growth factor

Based on the GF difference of water-soluble components (WSOM and AN) shown in Fig. 1, we assume the aerosol hygroscopicity is completely from AN component rather than WSOM. We select the ammonium nitrate as the representative of hygroscopic inorganic salts mixed with fine-mode aerosol water (AW_f) to estimate the growth factor (GF) of aerosol hygroscopicity in the fine mode. Tang (1996) observed the relationship of ammonium nitrate between the solute

Table 1
Complex refractive indexes ($m = n - ik$) and effective density (ρ) of typical particulate components. Real and imaginary parts at four standard AERONET aerosol product wavelengths (440, 675, 870 and 1020 nm) are considered.

		Real Part				Imaginary Part				ρ^a ($g\ cm^{-3}$)	References about CRI
		n_{440}	n_{675}	n_{870}	n_{1020}	k_{440}	k_{675}	k_{870}	k_{1020}		
OM	WIOM	1.530	1.530	1.530	1.530	0.035	0.001	0.001	0.001	1.0	Sun et al., 2007; Chen and Bond, 2010
	WSOM	1.530	1.530	1.530	1.530	0.006	0.000	0.000	0.000		
AN		1.559	1.553	1.550	1.548	0.000	0.000	0.000	0.000	1.73	Schuster et al., 2005
BC		1.950	1.950	1.950	1.950	0.790	0.790	0.790	0.790	2.0	Bond and Bergstrom, 2006
AW		1.337	1.332	1.330	1.328	0.000	0.000	0.000	0.000	1.0	Schuster et al., 2005
DU		1.534	1.534	1.534	1.534	0.002	0.001	0.001	0.001	2.3	Koven and Fung, 2006

[a] Zhang et al., 1993.

mass concentration and water activity as follows:

$$a_w = 1 + \sum_{k=1}^{4} C_k x^k \tag{5}$$

$$\rho_s(x) = 0.9971 + \sum_{k=1}^{4} A_k x^k \tag{6}$$

where x is the AN weight percent, a_w is the water activity, ρ_s is the solution density, C_k and A_k is the polynomial coefficient (values listed in Table 1 in Tang, 1996) and k is the polynomial order number. In practice, the water activity is close to the relative humidity (RH) due to lower curvature effect (Tang, 1996) with the form of percentage from the conventional meteorological observation,

$$RH \approx a_w/100 \tag{7}$$

The relative proportion of AN and AW can be calculated by Eq. (5) and Eq. (6) with the information on RH (Eq. (5)).

$$\frac{f_{AN}}{\left(f_{AN} + f_{AW_f}\right)} = x \cdot \frac{\rho(x)}{\rho(100.0)} = \frac{1}{GF^3(RH)} \tag{8}$$

where f_{AN} and f_{AW_f} represent the volume percent of AN and AW_f, respectively.

2.2.4. The separation between WSOM and AN depended on hygroscopic difference

In section above, the water-soluble and water-insoluble matters are separated by Eqs. (3) and (4) firstly, secondly the proportion of AN and AW_f are estimated by the significantly hygroscopicity (Eqs. (5)–(8)). And then, the WSOM component is mixed to obtain the entire aerosol water-soluble matter. Considering the complexity in the multi-component liquid mixture system, the volume averaged mixing rule (Heller, 1965) is employed to calculate the mixing CRI of WSOM, AN and AW,

$$m_e(\lambda) = \frac{\sum_j m_j(\lambda) f_j}{\sum_j f_j} \quad j = AN, AW_f \text{ and } WSOM \tag{9}$$

where, m_e is the CRI of the entire solution, m_j is the CRIs of WSOM, AN and AW components (Table 1), and f_j represents the volume percent of components. Noted that the refractive index of WSOM in a host liquid calculated by volume averaged mixing rule may be lower than that in the multicomponent liquid mixture system and brings in some uncertainty.

2.2.5. The separation between WIOM and BC depended on spectral difference

In the scheme, the brown carbon is regarded as a part of OM component which is spectrally light-absorbing component. Therefore, the mixing WIOM spectral behavior of weak light-absorbing characteristics can be distinguished although it is generally reduced by light-scattering OM (Kirchstetter et al., 2004). On the contrary, BC component shows the weak spectral changes but strong light-absorbing property which can be used to separate the WIOM from BC components. We choose the internal mixing method of Maxwell Garnett effective medium approximation (Schuster et al., 2005), and put the water-insoluble matters (BC and WIOM) as inclusion and water-soluble matters (AN, AW_f and WSOM) as their environment to calculate the mixture complex refractive index (m_f) as follows:

$$m_f(\lambda) = \sqrt{\frac{|\varepsilon_{eff}(\lambda)| + Re(\varepsilon_{eff}(\lambda))}{2}} + i\sqrt{\frac{|\varepsilon_{eff}(\lambda)| - Re(\varepsilon_{eff}(\lambda))}{2}} \tag{10}$$

where, ε_{eff} is the effective permittivity. Mixture effective permittivities are represented by the following formula:

$$\varepsilon_{eff}(\lambda) = \varepsilon_e + 3\varepsilon_e \left[\frac{\sum_j \frac{\varepsilon_j(\lambda) - \varepsilon_e(\lambda)}{\varepsilon_j(\lambda) + 2\varepsilon_e(\lambda)} f_j}{1 - \sum_j \frac{\varepsilon_j(\lambda) - \varepsilon_e(\lambda)}{\varepsilon_j(\lambda) + 2\varepsilon_e(\lambda)} f_j} \right] \quad j=BC \text{ and } WIOM \tag{11}$$

where, f_j is the fraction of volume percent of inclusion and N is the number of aerosol components. $\varepsilon_j(\lambda)$ and $\varepsilon_e(\lambda)$ are the permittivities of inclusion and its environment, respectively, which can be calculated by m_j listed in Table 1 and m_e using Eq. (10).

2.2.6. Estimated aerosol water content in coarse mode

Aerosol water content is not only in fine mode but also in coarse mode such as the small fog droplet (Hammer et al., 2014), and the aerosol water content can be more than 90% in the fog droplet. Therefore, the AW is also considered in the coarse mode and roughly estimated according to complex refractive index of coarse mode components as follows:

$$m_c(\lambda) = \frac{\sum_j m_j(\lambda) f_j}{\sum_j f_j} \quad j=DU \text{ and } AW_c \tag{12}$$

where, $m_j(\lambda)$ is complex refractive index and f_j is the volume percent in coarse mode, respectively. DU and AW_c denotes dust and aerosol water in coarse mode. $m_c(\lambda)$ is the mixing CRI in coarse mode and λ is the wavelength. In practical computation, we use Eq (12) to estimate the AW_c when the RH is more than 40%, and only use the imaginary part (k_c) of CRI at 675 nm due to significant difference of imaginary part between AW and DU (Table 1) and uncertainties of the real part of CRI in coarse mode (Zhang et al., 2017). The aerosol components of DU and AW_c can be directly solved by eq (12) combining with the law of substance conservation without the iteration process.

2.3. The aerosol component remote sensing scheme

We show the entire scheme procedure of aerosol component estimation in Fig. 3. As mentioned above, the AERONET CRIs are separated into fine and coarse modes described in Zhang et al. (2017), and then the aerosol components are estimated by the aerosol component

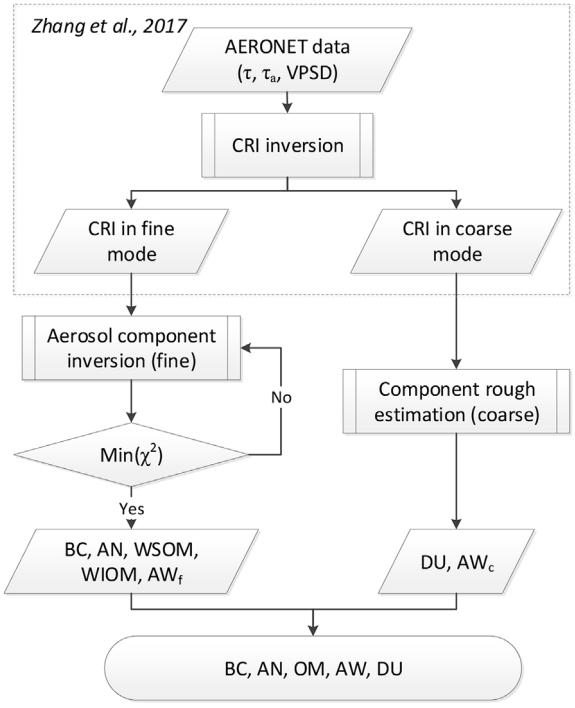

Fig. 3. Flowchart of the algorithm solution procedure. The first part in the box of dash line is described in the study of Zhang et al. (2017) in detail.

Table 2
Ratio (β) of water-soluble organic matter (WSOM) mass concentration in total OM.

period	β = WSOC/OC(%)			site	D (μm)	References
	Avg.	Min.	Max.			
2004.07-2007.02	44	17.5	71.3	Eastern Mediterranean Finokalia (35°32′N, 25°67′E)	8.39	Bougiatioti et al., 2013
1998.07-1998.08	55	31.5	66.7	Jungfraujoch high-alpine research station (46°33′ N, 7°59′ E; 3580 m)	2.5	Krivácsy et al., 2001
1999.10	66	50.2	83.0	Fazenda Nossa Senhora Aparecida (10°45′44″S, 62°21′27″W, 315 m)	2.5	Mayol-Bracero et al., 2002
1996.07-1996–10	77	69.2	95.2	Aspvreten (58°48′N, 17°23′E)	10.0	Zappoli et al., 1999
	48	47.8	50.0	K-puszta (46°58′N, 19°33′E, 130 m)		
	65	54.9	79.6	San Pietro Capoþume (44°39′N, 11°37′E, 10 m)		
2012.12-2014.11	25	17.8	28.4	Little Rock, Arkansas (Southern Mississippi Valley)	TSP	Chalbot et al., 2016
2010.10-2010.11	11	5.0	16.3	Eastern North Atlantic from the 2010 US GEOTRACES cruise (Except Mar1-3 sampling)	TSP	Wozniak et al., 2013

estimation scheme described in section 2.2. In this section, we mainly introduce the two constraints of iteration in fine mode and aerosol volume normalization.

2.3.1. Iteration of fine mode components

Although the mixture CRI of the liquid part in aerosol can be calculated following Eq. (9), in the process of the real inversion, the uncertainties increase significantly with the increase in numbers of components. In order to constrain the inversion, a relationship between WSOM and WIOM is used and the ratio of WSOM mass concentration to the total OM (called β hereafter) are listed in Table 2. Generally, β ranges from 44% to 77%, but can extend from 17.8% (Chalbot et al., 2016) to 95.2% (Zappoli et al., 1999) in the extreme cases. The observation of Wozniak et al. (2013), which presents the minimum of β is 5%, is not referred in this study because of the excessive clean condition over ocean. Therefore, we propose a relationship between volume percent of WSOM and WIOM components using the ratio β based on the hypothesis of approximate effective densities of the WSOM and WIOM:

$$\begin{cases} f_{WSOM} \cong \alpha \cdot f_{WIOM} \\ \alpha = \frac{\beta \rho_{WSOM}^{-1}}{1-\beta \rho_{WSOM}^{-1}} \end{cases} \quad \beta \in [44\%,\ 77\%] \tag{13}$$

Moreover, if $\alpha > f_s/f_i$, which the water-soluble matter ratio of OM is more than the entire aerosol, the range of β is extended to [17.8%, 95.2%].

Based on Eq. (13), the range of WSOM volume percent can be calculated by f_{WIOM}, and then the m_f can be obtain using Eq (10) with the changes of BC and WIOM. The differences in multiple wavelengths between mixing CRI (m_f) from Eq (10) and separated one ($m_{f,inv}$) according to Zhang et al. (2017) are chosen as the Chi-square (χ^2) of iterative kernel function to solve the equation and derive the volume percent of aerosol components:

$$\chi^2 = \sum_{\lambda} \frac{m_{f,inv}(\lambda) - m_f(\lambda)}{m_{f,inv}(\lambda)} \quad \lambda = 440,\ 675,\ 870 \text{ and } 1020 \text{ nm} \tag{14}$$

Moreover, the retrievals are further filtered with additional constraint which is the differences between fit and input real parts of CRIs at 440 nm are less than 0.05.

2.3.2. Constraint by normalization of aerosol volume

In this study, the aerosol volume normalization is used to constrain the volume percent of aerosol components into a reasonable range. The total volume percent of aerosol is sum of that in fine and coarse mode (f_{fine} and f_{coarse}) calculated by VPSD, and the modal volume percent (f_{fine} and f_{coarse}) is sum of that of aerosol components in the fine and coarse mode, respectively (Eq (15)).

$$\begin{cases} f_{fine} + f_{coarse} = 1.0 \\ f_{fine} = f_{BC} + f_{AN} + f_{WSOM} + f_{WIOM} + f_{AW_f} \\ f_{coarse} = f_{DU} + f_{AW_c} \end{cases} \tag{15}$$

And then, the volume or mass concentrations of aerosol components can be obtained by which multiplied by aerosol entire volume and effective densities.

2.4. Uncertainty estimation of OM

The uncertainties in the estimated aerosol components can be derived from CRI, VPSD and RH. The CRI uncertainty caused by mixed component (e.g. OM) has been estimated by Schuster et al. (2015) and changes from 50% to 440%. Li et al. (2013) shows the OM component error from the input CRIs is nearly 80% and that of other components range from 30% to 140% in a case study. For VPSD, the error in different aerosol type is about 25% ± 10% (Dubovik et al., 2000). Further, the uncertainties from RH are discussed in this study (Fig. 4). Analyzing the aerosol component estimation scheme, the theoretical errors induced by RH are mainly affected from (i) the separation between water-soluble and water-insoluble matters (f_i/f_s), (ii) the estimation of proportion of AN (f_{AN}), and (iii) the inherent uncertainty of the $\psi(RH)$.

The uncertainty of f_i/f_s can be obtained by derivation of $\psi(RH)$ in Eq (3) because the integral of ε keeps constant for fixed aerosol type and size range. Fig. 4(a) shows the $\psi(RH)$ and its absolute and relative errors with the RH error of 5% (WMO, 2008) in the condition of $f_i + f_s = 1.0$. The absolute error of $\psi(RH)$ is reduced to less than 0.84 in the range of RH from 1% to 99%. But the relative error is increased with peak value of 66% (RH = 85%), and then decreased when RH > 85%. The mean error is about 31.6% when the RH is no more than 85%.

The uncertainty of f_{AN} with the RH range from 27% to 99% in the condition of $f_{AN} + f_{AW_f} = 1.0$ is shown in Fig. 4(b). The absolute error of f_{AN} is increased and even larger than itself, thus the relative error is dramatically increased over 100% when the RH is more than 95%. Considering the algorithm is intended to retrieve the aerosol components without cloud and fog, the relative error can be less than 30.1%, with the mean error of 10.6% corresponding to RH less than 85%.

The inherent uncertainty of the $\psi(RH)$ is also estimated by employing the observed growth rate of sulfate (0.18) and primary organic matter (0.009) with *RH* applied to water-soluble and water-insoluble components respectively, which are observed in Beijing from 21

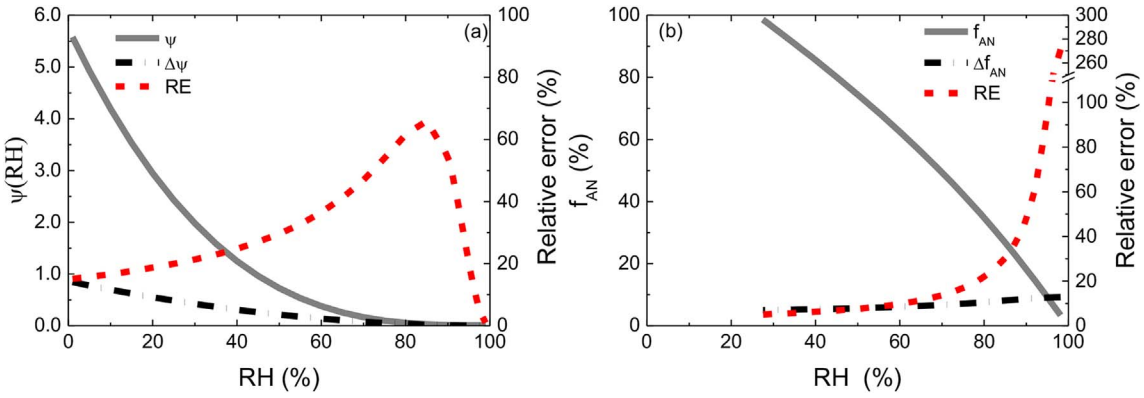

Fig. 4. Errors of the re-parameterized function (ψ) and volume percent of AN component (f_{AN}). The solid line represents the values of ψ and f_{AN}; the dash dot and dash lines represent the absolute and relative errors corresponding to the left and right y-axes, respectively. The Δ and RE in the figure are calculated by $\Delta = \frac{\delta Y}{\delta RH} \cdot 5\%$ and $RE = \frac{\Delta}{Y}$. Y represents the ψ or f_{AN}, and δY represents the change of Y with δRH.

November 2011 to 20 January 2012 by Sun et al. (2013). Based on the growth rates, the increase of water-soluble and water-insoluble components with RH can be estimated with the initial proportion of 1:1 and initial RH of 20%. The estimated average relative error of $\psi(RH)$ is 57.4% with the range from 4.2% to 95.8%.

Through the synthesis above errors, we choose the averaged errors for each source and calculated the range using the maximum and minimum errors as listed in Table 3. The propagation error of OM component is about 106.9%, with the range from about 62.4% to 478.4%. It should be noted that this estimation of uncertainty is for single measurement. One of important advantage of remote sensing approach is to perform multiple measurements quickly in a short time period. Furthermore, considering the uncertainty of the daily OM, assuming independent errors in each observation, the average uncertainty in OM ($\Delta\overline{OM}$) can be given by (Li et al., 2008):

$$\Delta\overline{OM} = \frac{1}{N_t}\left[\sum_{N_t}(\Delta OM(t))^2\right]^{\frac{1}{2}}, \quad (16)$$

where, the N_t is the number of the OM observations. If the error in each record is about the same, Eq. (16) can be simplified to $N_t^{-\frac{1}{2}}\Delta OM(t)$. Usually, there are more than four observations in a day, that means the uncertainty of daily OM can be less than about 50%.

3. Results

3.1. Measurements

We use the AERONET (Holben et al., 1998) data including τ (aerosol optical depth), τ_a (absorbing τ), and VPSD (volume particle size distribution) at Beijing site (Beijing_RADI, 40.01 °N, 116.38 °E, 59.0 m a. s. l.) from October of 2014 to January of 2015. The Lev 1.5 data used (due to no lev 2.0 exist) in this study is further filtered with strong quality control criteria as suggested by AERONET (Holben et al., 2006) including (1) solar zenith angles > 50°, (2) the minimum number of observation angles specified by AERONET Lev 2.0 data criteria, and (3) the total retrieval residual less than 5%. Moreover, the extra quality control of AOD (440 nm) > 0.4 is applied to τ_a. AERONET data is used to separate the CRI into fine and coarse mode, and then executing aerosol components estimation as inputs.

The ambient relative humidity (RH) is observed by the automatic meteorological station at Beijing_RADI site. In order to analyze the ground surface observations, the planet boundary layer height (PBLH) from lidar observations (Mortier et al., 2016; Zhang et al., 2014) at the same site are also used to obtain the aerosol concentration profile (Zhang et al., 2015). Particulate matter mass concentrations ($PM_{2.5}$ and PM_{10}, aerodynamic diameter less than 2.5 and 10 μm, respectively) are observed coincidently by MetOne BAM-1020 p.m. monitors with $PM_{2.5}$ and PM_{10} cutting head in order to distinguish the pollution events.

Fig. 5 shows the meteorological factors (RH and PBLH) and particle mass concentration ($PM_{2.5}$ and PM_{10}) changes from Oct of 2014 to Jan 2015. The RH, $PM_{2.5}$ and PM_{10} are processed for the daily average, while the PBLH data is the average of daytime due to the degradation of the boundary layer at night. The RH presents a decrease trend from October to December of 2014, and a slight increase in January of 2015. The diurnal PBLH changes largely from 0.3 to 2.7 km, and valley values correspond to the peak of particle mass concentrations. Daily $PM_{2.5}$ and PM_{10} present the similar trend including several haze pollution events, with the mean values of 111 and 155 μg m^{-3}, respectively.

3.2. Columnar aerosol components in Beijing

Fig. 6 shows the retrieved mass concentrations of aerosol components in the atmospheric column based on ground-based remote sensing observations from October of 2014 to January of 2015. Retrieved OM (WSOM and WIOM) is widely found in aerosols in the experiment period, with the mean mass concentration of 58.6 mg m^{-2}, accounting for 14.93% in the total aerosol mass (Table 4). More specifically, WSOM component rapidly increases in polluted condition, but WIOM is relatively stable. The mean of WSOM and WIOM components account for

Table 3
Total errors of OM components from CRI, VPSD and RH sources.

Error (%)	CRI		VPSD	RH		ψ	Total[a]
	Mixed component	Input CRI		f_i/f_s	Hygroscopicity	Inherent	
mean	–	80	25	31.6	10.6	57.4	106.9
Minimum	50.0	30	15	15.1	5.1	4.2	62.4
maximum	440.0	140	35	66	30.1	95.8	478.4
Reference	Schuster et al., 2015	Li et al., 2013	Dubovik et al., 2000	This study	This study	This study	This study

[a] Total = $\sqrt{\sum_{i=1}^{6} x_i^2}$.

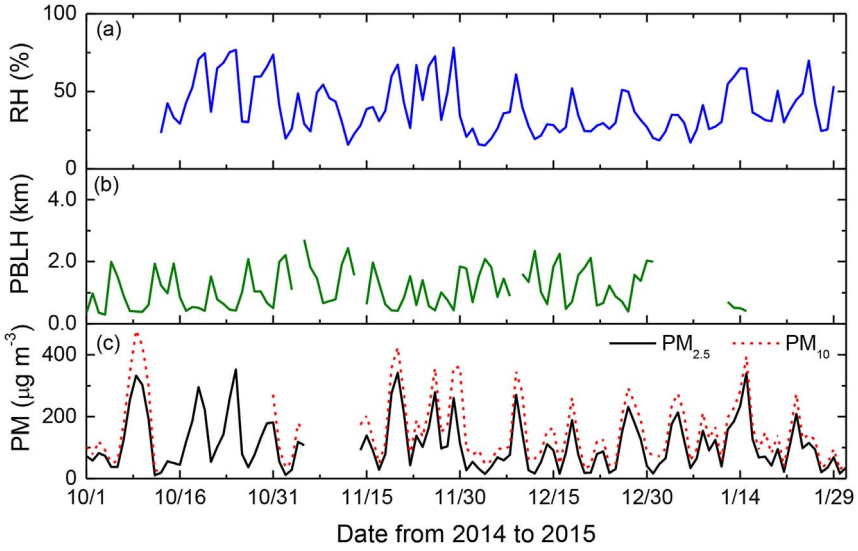

Fig. 5. The variations of daily relative humidity (RH), planetary boundary layer height (PBLH), $PM_{2.5}$ and PM_{10} from October 2014 to January 2015.

7.31 and 7.63%, respectively. The AN component presents the large changes due to the serious pollution event especially on 24th and 25th October of 2014, corresponding to daily $PM_{2.5}$ concentration up to 332 μg m^{-3} (24th October). Thus, the maximum percentage of AN component is up to 16.94% in the October, while less than 12% in the other months. BC concentrations in aerosol increase from 3.2 mg m^{-2} in October to 5.5 mg m^{-2} in January, with the maximum daily mean of 7.3 mg m^{-2} on January 3rd, 2015. The change of AW (i.e. AW_f and AW_c) consists with AN component, with a proportion of 3.77% averaged in the experiment period due to the low humidity in winter. The percentage of AW_f in October is significantly larger than that in other months because of the relatively high RH (47.69%) which averaged at the moments of ground-based remote sensing measurements. However, there is hardly any percentage of AW_c in winter, except on 18th December. These results indicate that water uptake in fine mode is mainly influenced by RH, while the water content in coarse mode could be impacted by complex mechanism. If only pay attention to the dry aerosol components in fine mode, the OM, AN and BC account for 51.24%, 46.31% and 2.46%, respectively. The dust component is dominant in total aerosols with the mean percentage of 69.72%, more than ground-based observation ($[PM_{10}\text{-}PM_{2.5}]/PM_{2.5}$ = 35.2%), maybe explained by the fine-mode aerosol concentration less than $PM_{2.5}$. In addition, the percentage of dust can be lower than 50% in heavy

Table 4
Monthly percentages of aerosol component mass concentrations in atmospheric column in Beijing from October 2014 to January 2015.

Month	OM %		AN %	BC %	AW %		DU %	RH %
	WSOM	WIOM			AW_f	AW_c		
2014–10	4.88	4.58	16.94	0.52	7.42	0.00	65.66	47.69
2014–11	5.57	7.34	11.19	0.85	3.92	0.00	71.14	47.75
2014–12	10.58	7.33	6.29	1.63	0.87	1.32	71.98	29.06
2015–01	9.48	9.97	7.56	1.31	1.57	0.00	70.11	41.37
Mean	7.63	7.31	10.50	1.08	3.44	0.33	69.72	41.46
	14.93				3.77			

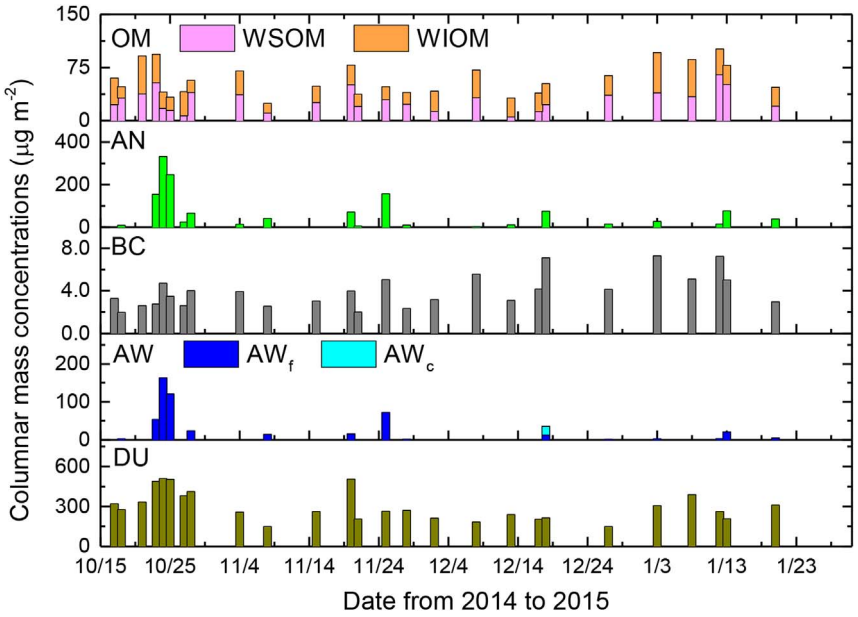

Fig. 6. Daily mass concentration variation of aerosol components in atmospheric column in Beijing from October 2014 to January 2015.

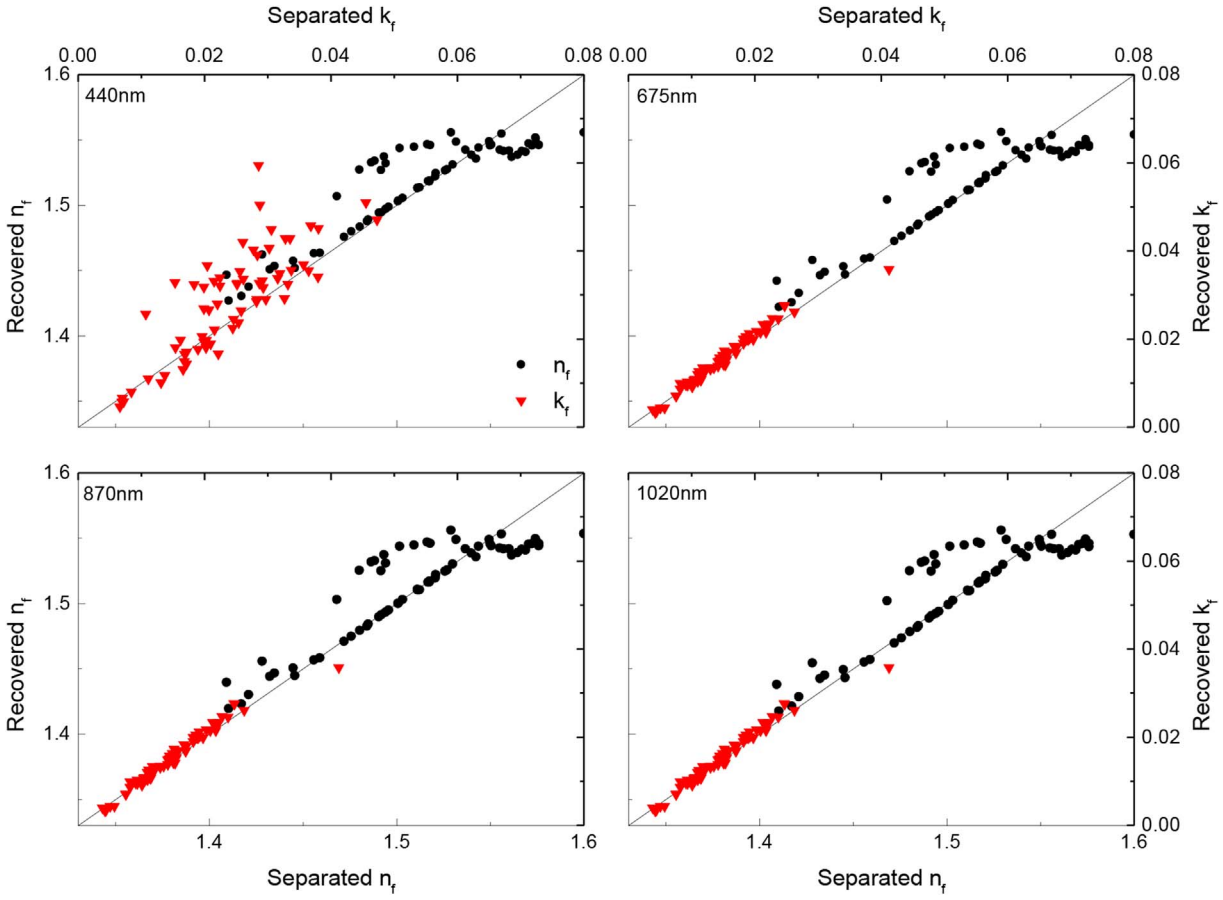

Fig. 7. Recovery of CRI (n_f and k_f) based on the aerosol component estimation in fine mode (N = 568). The four panels correspond to different wavelengths (440, 675, 870 and 1020 nm).

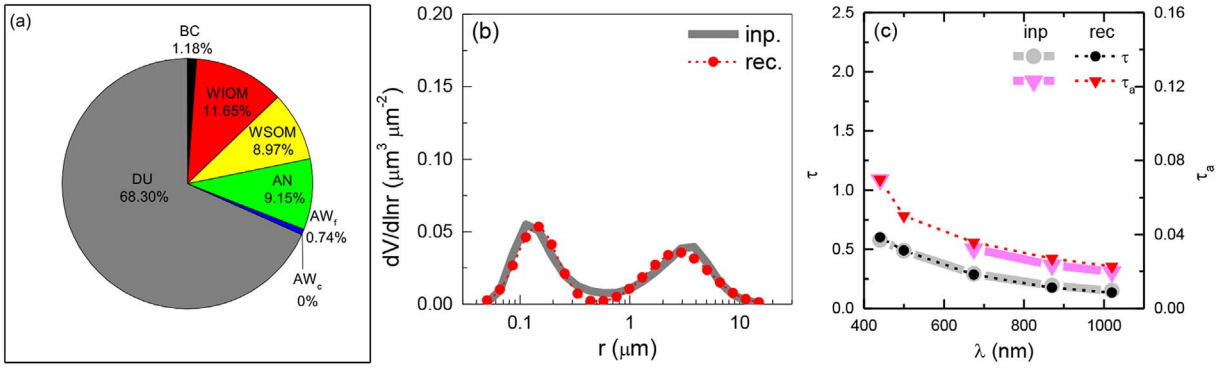

Fig. 8. (a) The mass percent of aerosol components including BC, WIOM, WSOM, AN, AW_f, AW_c and DU, and recovered (b) VPSD, (c) τ and τ_a mixed by aerosol components in non-haze case (2014.11.08 15:52:14). In the figures (b) and (c), "inp" and "rec" is the input and recovered parameters, respectively.

polluted conditions.

In Fig. 7, we illustrate the recovery of separated CRI in fine mode (n_f and k_f). It can be seen that the averaged bias of real part of CRI (n_f) is lower than 0.016 at each wavelength due to its weak changes with wavelength. The averaged biases of k_f are only about 0.001 at 675, 870 and 1020 nm, but the maximum occurs at 440 nm with the mean of 0.006. This large bias can be explained by the overestimation of imaginary part of OM mixtures at 440 nm. However, the imaginary part of OM mixture at 440 nm can be changed with its compositions (Kirchstetter et al., 2004; Nakayama et al., 2013) and difficult to be estimated, e.g. the concentration changes of brown carbon due to biomass burning. It is suggested that the imaginary part of CRI at 440 nm can be reduced its weight in the iteration or improved its accuracy in the future.

3.3. Comparisons with in situ measurements

The aerosol chemical components in PM_1 are measured by a High-Resolution Aerosol Mass Spectrometer (HR-AMS) at ground level from 15 October to 13 November 2014 (Sun et al., 2016) to compare with the OM based on remote sensing. In order to obtain the remotely sensed aerosol components near the surface, the uniform vertical distribution

can be assumed (Chu et al., 2013) and parameterized with planet boundary layer height (PBLH) (Zhang et al., 2014) to convert the aerosol components in column to near the ground. For comparable species, we choose the observed organics to compare with the OM, and the sum of sulfate, nitrate and ammonium to compare with the AN. Firstly, we choose the non-haze (2014.11.08 15:52:14) and haze (2014.10.23 15:00:56) cases with different relative humidity (54% vs 68%) and similar boundary layer (664 m vs 638 m) to analyze the mass percent of aerosol components and corresponding optical fit results, compared with in situ aerosol chemical components. And then the mass concentrations of OM, AN and BC components near the surface based on remote sensing are compared with in situ measurements.

Fig. 8 shows the remotely sensed mass percent of aerosol components, the fit CRIs rebuilt by aerosol components, and fit results of VPSD, τ and τ_a in non-haze case. In non-haze case, the fraction of dust-like aerosol dominates the total mass and accounts for 68.30%. The mass percent of OM is second-most and includes WIOM of 11.65% and WSOM of 8.97% (Fig. 8(a)). The AN component is relatively low with the mass percent of 9.15%. AW fraction in fine mode is about 0.74% and none AW in coarse mode due to the low RH. The mass percent of OM and AN in fine-mode dry aerosol from remote sensing is 66.63% and 29.55%, respectively, close to the in situ observations of 52.83% and 43.21%. The BC component is close to the in situ measurement in PM_1 (3.81 vs 3.96%), indicating that the BC in fine mode can be concentrated in PM_1 in non-haze day.

Correspondingly, the recovered properties are analyzed in terms of optical and microphysical parameters including VPSD and optical parameters (τ and τ_a). Compared with the input VPSD from AERONET, the sum of VPSD errors is 0.081 $\mu m^3/\mu m^2$ introduced by separation process in non-haze cases, with the mean relative errors of 23.08% except the first and last bins (Fig. 8(b)). The optical fit results (τ and τ_a) is fairly good consisted with the input data. The mean relative errors are 5.83% for τ, and 7.91% for τ_a in non-haze cases (Fig. 8(c)).

On the contrary, Fig. 9(a) shows AW mass percent significantly increases from 0.74 to 6.78% in haze case. The secondly important increase of AN component is up to 19.45%. The mass percent of WSOM component shows a tiny decrease about 2.22%, while that of WIOM reduces obviously. Moreover, the mass percent of BC and DU are also decreased. The mass percent of OM (37.35 vs 33.86%) and AN (61.55 vs 60.98%) are very close to the in situ measurements, while the lower BC mass percent is reasonable because BC components is more likely in PM_1. In haze case, the sum of VPSD error is 0.084 $\mu m^3/\mu m^2$, with the mean relative error of only 7.12% (Fig. 9(b)). And the optical fit results (τ and τ_a) is fairly good consisted (1.21 and 9.40%) with the input data (Fig. 9(c)).

Fig. 10 shows the comparison of OM, AN and BC components between observation and remote sensing at the corresponding observation moments. The trend of estimated OM is consistent with the observed OM. Particular to polluted period, the estimated OM mass concentration peaks on October 24th and 25th 2014, in accordance with observed OM and $PM_{2.5}$ (Fig. 5). A fairly good correlation can be found between estimated and observed OM (R = 0.59). The correlation of AN component is better than that of OM, with the correlation coefficient of up to 0.89. The BC from remote sensing algorithm is also a good correlation (R = 0.73) with observation. The aerosol component errors can be derived from the uncertainties of in situ measurements, and also explained by different aerosol size between estimated and observed OM in fine mode and PM_1, respectively.

4. Conclusions and discussions

Based on separated aerosol physical properties into fine and coarse mode, we develop the inversion algorithm of OM component using the differences of aerosol hygroscopicities. The species of aerosol are classified five components, including black carbon (BC), organic matter (OM), ammonium nitrate-like (AN), dust-like (DU) components and aerosol water content (AW). OM is further separated into water-soluble and water insoluble organic matter (WSOM and WIOM), and AW also be separated into fine- and coarse-mode AW (AW_f and AW_c). Aerosol components are retrieved in Beijing using the AERONET measurements of Beijing RADI site from October of 2014 to January of 2015, compared with the chemical analysis. Results show that the retrieval algorithm of aerosol components has good ability and low fit error of CRIs. During the experiment period, columnar OM mass concentration accounts for 14.93% in total aerosol, and 56.34% in dry and fine-mode aerosol based on remote sensing, suggested that OM is also an important component in fine-mode aerosol. Compared with chemical analysis results, retrieved OM concentrations from remote sensing are close to observations near the ground, with the correlation coefficient of 0.56.

The OM inversion algorithm is driven by the aerosol spectral refractive indices of both fine and coarse modes. The use of AERONET retrievals as the inputs in this paper is only a demonstration for the application to the entire columnar atmosphere, though suffering from larger uncertainties associated with input refractive indices themselves. The more accurate input aerosol refractive indices (e.g. those from in situ measurement approaches) the better estimated OM results can be expected. Meanwhile, although a simple method of the coarse-mode aerosol water content has been added, the relatively low accuracy of inversion algorithm in coarse mode still exists. The OM component in coarse mode (e.g. fungus and spore) are not involved in the inversion algorithm, also increasing the uncertainties of inversion algorithm. In the future, the retrievals of aerosol components will be improved by upgrading the accuracy of CRI, considering the coarse-mode OM and involving in both the hygroscopic growth and cloud process for water-soluble inorganic salts. Moreover, the brown carbon included in the OM can be further distinguished with its spectral dependence (Schuster et al., 2015; Wang et al., 2013).

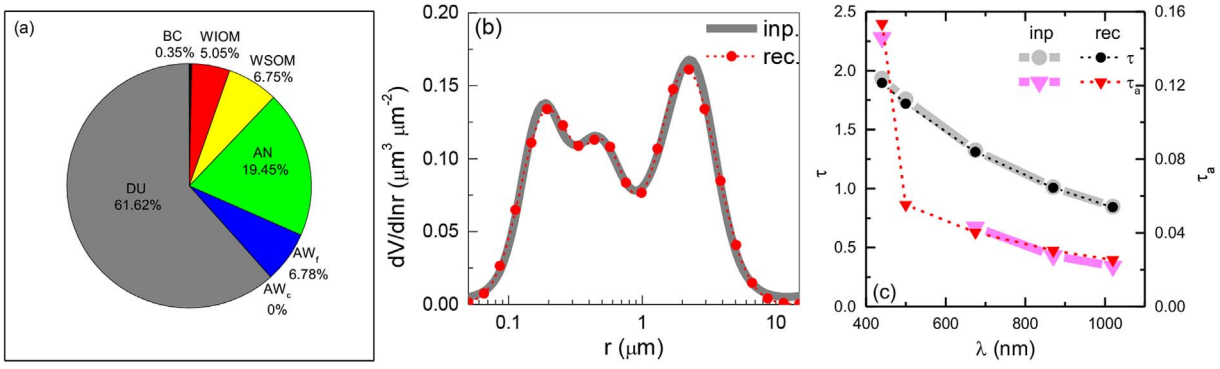

Fig. 9. Same as Fig. 8, except in haze case (2014.10.23 15:00:56).

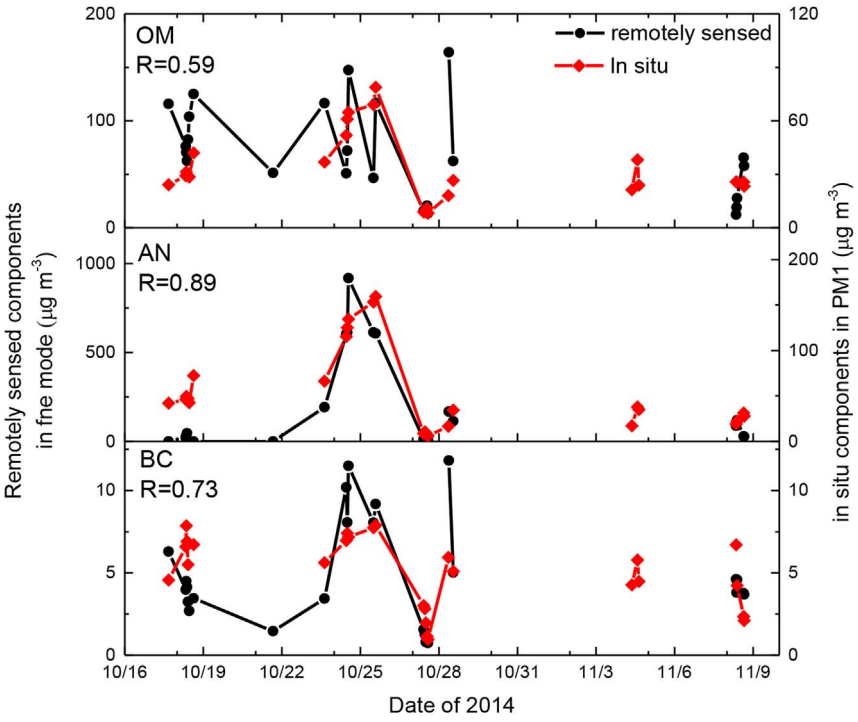

Fig. 10. OM, AN and BC retrieved by remote sensing compared with OM in PM_1 based on in situ measurements near the surface. Black line represents the estimated components from remote sensing, and red one is the observed components. (For interpretation of the references to colour in this figure legend, the reader is referred to the Web version of this article.)

Acknowledgement

This work was supported by the National Key R&D Program of China (2016YFE0201400) and the National Natural Science Fund of China (No. 41601386, 41671367 and 91544219).

References

Andreae, M.O., Gelencsér, A., 2006. Black carbon or brown carbon? the nature of light-absorbing carbonaceous aerosols. Atmos. Chem. Phys. 6 (10), 3131–3148.
Arola, A., Schuster, G., Myhre, G., Kazadzis, S., Dey, S., Tripathi, S.N., 2011. Inferring absorbing organic carbon content from AERONET data. Atmos. Chem. Phys. 11 (1), 215–225.
Bond, T., Bergstrom, R., 2006. Light absorption by carbonaceous particles: an investigative review. Aerosol. Sci. Technol. 40, 27–67.
Boucher, O., Randall, D., Artaxo, P., Bretherton, C., Feingold, G., Forster, P., Kerminen, V.-M., Kondo, Y., Liao, H., Lohmann, U., Rasch, P., Satheesh, S.K., Sherwood, S., Stevens, B., Zhang, X.Y., 2013. Clouds and aerosols. In: Stocker, T.F., Qin, D., Plattner, G.-K., Tignor, M., Allen, S.K., Boschung, J., Nauels, A., Xia, Y., Bex, V., Midgley, P.M. (Eds.), Climate Change 2013: the Physical Science Basis. Contribution of Working Group I to the Fifth Assessment Report of the Intergovernmental Panel on Climate Change. Cambridge University Press, Cambridge, United Kingdom and New York, NY, USA.
Bougiatioti, A., Zarmpas, P., Koulouri, E., Antoniou, M., Theodosi, C., Kouvarakis, G., Saarikoski, S., Mäkelä, T., Hillamo, R., Mihalopoulos, N., 2013. Organic, elemental and water-soluble organic carbon in size segregated aerosols, in the marine boundary layer of the Eastern Mediterranean. Atmos. Environ. 64, 251–262.
Cao, J.J., Lee, S.C., Ho, K.F., Zhang, X.Y., Zou, S.C., Fung, K., Chow, J.C., Watson, J.G., 2003. Characteristics of carbonaceous aerosol in Pearl River Delta Region, China during 2001 winter period. Atmos. Environ. 37, 1451–1460.
Cao, J.J., Lee, S.C., Ho, K.F., Zou, S.C., Fung, K., Li, Y., Watson, J.G., Chow, J.C., 2004. Spatial and seasonal variations of atmospheric organic carbon and elemental carbon in Pearl River Delta Region, China. Atmos. Environ. 38, 4447–4456.
Cao, J.J., Lee, S.C., Chow, J.C., Watson, J.G., Ho, K.F., Zhang, R.J., Jin, Z.D., Shen, Z.X., Chen, G.C., Kang, Y.M., Zou, S.C., Zhang, L.Z., Qi, S.H., Dai, M.H., Cheng, Y., Hu, K., 2007. Spatial and seasonal distributions of carbonaceous aerosols over China. Journal of Geophysical Research Atmospheres 112, D22S11.
Chan, C.K., Yao, X., 2008. Air pollution in mega cities in China. Atmos. Environ. 42, 1–42.
Chalbot, M.G., Chitranshi, P., da Costa, G.G., Pollock, E., Kavouras, I.G., 2016. Characterization of water-soluble organic matter in urban aerosol by ^{1}H-NMR spectroscopy. Atmos. Environ. 128, 235–245.
Chen, Y., Bond, T.C., 2010. Light absorption by organic carbon from wood combustion. Atmos. Chem. Phys. 10, 1773–1787.
Choi, Y., Ghim, Y.S., 2016. Estimation of columnar concentrations of absorbing and scattering fine mode aerosol components using AERONET data. J. Geophys. Res. Atmos. 121, 13628–13640.
Chu, D.A., Tsai, T.-C., Chen, J.-P., Chang, S.-C., Jeng, Y.-J., Chiang, W.-L., Lin, N.-H., 2013. Interpreting aerosol lidar profile to better estimate surface PM2.5 for columnar AOD measurements. Atmos. Environ. 79, 172–187.
Cuesta, J., Flamant, P.H., Flamant, C., 2008. Synergetic technique combining elastic backscatter lidar data and sun photometer AERONET inversion for retrieval by layer of aerosol optical and microphysical properties. Appled Optics 47, 4598–4611.
Dubovik, O., Smirnov, A., Holben, B.N., King, M.D., Kaufman, Y.J., Eck, T.F., Slutsker, I., 2000. Accuracy assessments of aerosol optical properties retrieved from aerosol robotic network (AERONET) Sun and sky radiance measurements. J. Geophys. Res. Atmos. 105, 9791–9806.
Hammer, E., Gysel, M., Roberts, G.C., Elias, T., Hofer, J., Hoyle, C.R., Bukowiecki, N., Dupont, J.C., Burnet, F., Baltensperger, U., Weingartner, E., 2014. Size-dependent particle activation properties in fog during the Paris Fog 2012/13 field campaign. Atmos. Chem. Phys. 14, 10517–10533.
Heller, W., 1965. Remarks on refractive index mixture rules. J. Phys. Chem. 69 (4), 1123–1129.
Holben, B.N., Eck, T.F., Slutsker, I., Smirnov, A., Sinyuk, A., Schafer, J., Giles, D., Dubovik, O., 2006. AERONET's version 2.0 quality assurance criteria remote sensing of atmosphere and clouds. Proc. SPIE-Int. Soc. Opt. Eng. 6408, 64080. http://dx.doi.org/10.1117/12.706524.
Holben, B.N., Eck, T.F., Slutsker, I., Tanre, D., Buis, J.P., Setzer, A., Vermote, E., Reagan, J.A., Kaufman, Y.J., Nakajima, T., Lavenu, F., Jankowiak, I., Smirnov, A., 1998. AERONET—a federated instrument network and data archive for aerosol characterization. Rem. Sens. Environ. 66, 1–16.
Hu, D., Qiao, L., Chen, J., Ye, X., Yang, X., Cheng, T., Fang, W., 2010. Hygroscopicity of inorganic aerosols: size and relative humidity effects on the growth factor. Aerosol Air Qual. Res. 10, 255–264.
Jing, B., Tong, S., Liu, Q., Li, K., Wang, W., zhang, Y., Ge, M., 2016. Hygroscopic behavior of multicomponent organic aerosols and their internal mixtures with ammonium sulfate. Atmos. Chem. Phys. 16, 4101–4118.
Kandler, K., Schütz, L., 2007. Climatology of the average water-soluble volume fraction of atmospheric aerosol. Atmos. Res. 83, 77–92.
Kirchstetter, T.W., Novakov, T., Hobbs, P.V., 2004. Evidence that the spectral dependence of light absorption by aerosols is affected by organic carbon. J. Geophys. Res. 109, D21208. http://dx.doi.org/10.1029/2004JD004999.
Krivácsy, Z., Gelencsér, A., Kiss, G., Mészáros, E., Molnár, Á., Hoffer, A., Mészáros, T., Sárvári, Z., Temesi, D., Varga, B., Baltensperger, U., Nyeki, S., Weingartner, E., 2001. Study on the chemical character of water soluble organic compounds in fine atmospheric aerosol at the jungfraujoch. J. Atmos. Chem. 39, 235–259.
Koven, C.D., Fung, I., 2006. Inferring dust composition from wavelength-dependent absorption in Aerosol Robotic Network (AERONET) data. J. Geophys. Res. 111, D14205. http://dx.doi.org/10.1029/2005JD006678.
Lafon, S., Rajot, J.-L., Alfaro, S., Gaudichet, A., 2004. Quantification of iron oxides in desert aerosol. Atmos. Environ. 38, 1211–1218.

Li, Z., Eck, T., Zhang, Y., Zhang, Y.H., Li, D., Li, L., Xu, H., Hou, W., Lv, Y., Goloub, P., Gu, X., 2014a. Observations of residual submicron fine aerosol particles related to cloud and fog processing during a major pollution event in Beijing. Atmos. Environ. 86, 187–192.

Li, K., Wang, W., Ge, M., Li, J., Wang, D., 2014b. Optical properties of secondary organic aerosols generated by photooxidation of aromatic hydrocarbons. Sci. Rep. 4, 4922. http://dx.doi.org/10.1038/srep04922.

Li, Z., Li, L., Zhang, F., Li, D., Xie, Y., Xu, H., 2015. Comparison of aerosol properties over Beijing and Kanpur: optical, physical properties and aerosol component composition retrieved from 12 years ground-based Sun-sky radiometer remote sensing data. J. Geophys. Res. 120, 1520–1535. http://dx.doi.org/10.1002/2014JD022593.

Li, Z., Gu, X., Wang, L., Li, D., Xie, Y., Li, K., Dubovik, O., Schuster, G., Goloub, P., Zhang, Y., Li, L., Ma, Y., Xu, H., 2013. Aerosol physical and chemical properties retrieved from ground-based remote sensing measurements during heavy haze days in Beijing winter. Atmos. Chem. Phys. 13, 10171–10183.

Li, Z., Blarel, L., Podvin, T., Goloub, P., Buis, J.-P., Morel, J.-P., 2008. Transferring the calibration of direct solar irradiance to diffuse-sky radiance measurements for CIMEL Sun–sky radiometers. Appl. Optic. 47 (10), 1368–1377.

Liu, Q., Jing, B., Peng, C., Tong, S., Wang, W., Ge, M., 2016. Hygroscopicity of internally mixed multi-component aerosol particles of atmospheric relevance. Atmos. Environ. 125, 69–77.

Mayol-Bracero, O.L., Guyon, P., Graham, B., Roberts, G., Andreae, M.O., Decesari, S., Facchini, M.C., Fuzzi, S., Artaxo, P., 2002. Water-soluble organic compounds in biomass burning aerosols over Amazonia 2. apportionment of the chemical composition and importance of the polyacidic fraction. Atmos. Chem. Phys. 107 (D20), 8091. http://dx.doi.org/10.1029/2001JD000522.

Mortier, A., Goloub, P., Derimian, Y., Tanré, D., Podvin, T., Blarel, L., Deroo, C., Marticorena, B., Diallo, A., Ndiaye, T., 2016. Climatology of aerosol properties and clear-sky shortwave radiative effects using Lidar and Sun photometer observations in the Dakar site. Atmos. Chem. Phys. 121, 6489–6510. http://dx.doi.org/10.1002/2015JD024588.

Nakayama, T., Sato, K., Matsumi, Y., Imamura, T., Yamazaki, A., Uchiyama, A., 2013. Wavelength and NOx dependent complex refractive index of SOAs generated from the photooxidation of toluene. Atmos. Chem. Phys. 13, 531–545.

Prenni, A.J., DeMott, P.J., Kreidenweis, S.M., 2003. Water uptake of internally mixed particles containing ammonium sulfate and dicarboxylic acids. Atmos. Environ. 37, 4243–4251.

Putaud, J.P., Raes, F., van Dingenen, R., Brüggemann, E., Facchini, M.-C., Decesari, S., Fuzzi, S., Gehrig, R., Hüglin, C., Laj, P., Lorbeer, G., Maenhaut, W., Mihalopoulos, N., Müller, K., Querol, X., Rodriguez, S., Schneider, J., Spindler, G., ten Brink, H., Tørseth, K., Wiedensohler, A., 2004. A European aerosol phenomenology - 2: chemical characteristics of particulate matter at kerbside, urban, rural and background sites in Europe. Atmos. Environ. 38, 2579–2595.

Satheesh, S.K., Srinivasan, J., 2002. Enhanced aerosol loading over Arabian Sea during the pre-monsoon season: natural or anthropogenic. Geophys. Res. Lett. 29 (18), 211–214.

Satheesh, S.K., Krishna, M.K., 2005. Radiative effects of natural aerosols: a review. Atmos. Environ. 39 (11), 2089–2110.

Satheesh, S.K., Ramanathan, V., Holben, B.N., Moorthy, K.K., Loeb, N.G., Maring, H., Prospero, J.M., Savoie, D., 2002. Chemical, microphysical, and rediative effects of Indian Ocean aerosols. J. Geophys. Res. 107 (D23), 4725.

Satheesh, S.K., Ramanathan, V., Li-Jones, X., Lobert, J.M., Podgorny, I.A., Prospero, J.M., Holben, B.N., Loeb, N.G., 1999. Amodel for the natural and anthropogenic aerosols over the tropical Indian Ocean derived from Indian ocean experiment data. J. Geophys. Res. 104 (D22), 27421–27440.

Saxena, P., Hildemann, L.M., 1996. Water-soluble organics in atmospheric particles: a critical review of the literature and application of thermodynamics to identify candidate compounds. Atmos. Chem. Phys. 24, 57–109.

Schuster, G.L., Dubovik, O., Arola, A., 2015. Remote sensing of soot carbon – Part 1: distinguishing different absorbing aerosol species. Atmos. Chem. Phys. 16, 1565–1585.

Schuster, G.L., Lin, B., Dubovik, O., 2009. Remote sensing of aerosol water uptake. Geophys. Res. Lett. 36, L03814. http://dx.doi.org/10.1029/2008GL036576.

Schuster, G.L., Dubovik, O., Holben, B.N., Clothiaux, E.E., 2005. Inferring black carbon content and specific absorption from Aerosol Robotic Network (AERONET) aerosol retrievals. J. Geophys. Res. 110, D10S17. http://dx.doi.org/10.1029/2004JD004548.

Shi, Y., Ge, M., Wang, W., 2012. Hygroscopicity of internally mixed aerosol particles containing bezoic acid and inorganic salts. Atmos. Environ. 60, 9–17.

Sjogren, S., Gysel, M., Weingartner, E., Baltensperger, U., Cubison, M.J., Coe, H., Zardini, A.A., Marcolli, C., Krieger, U.K., Peter, T., 2007. Hygroscopic growth and water uptake kinetics of two-phase aerosol particles consisting of ammonium sulfate, adipic and humic acid mixtures. J. Aerosol Sci. 38, 157–171.

Sun, H., Biedermann, L., Bond, T.C., 2007. Color of brown carbon: a model for ultraviolet and visible light absorption by organic carbon aerosol. Geophys. Res. Lett. 34, L17813. http://dx.doi.org/10.1029/2007GL029797.

Sun, Y., Zang, Z., Wild, O., et al., 2016. "APEC Blue": sencondary aerosol reductions from emission controls in Beijing. Sci. Rep. 6, 20668 (1-9).

Sun, Y., Wang, Z., Fu, P., Jiang, Q., Yang, T., Li, J., Ge, X., 2013. The impact of relative humidity on aerosol composition and evolution processes during wintertime in Beijing, China. Atmos. Environ. 77, 927–934.

Tang, I.N., 1996. Chemical and size effects of hygroscopic aerosol on light scattering coefficents. J. Geophys. Res. 101 (D14), 19245–19250.

Varutbangkul, V., Brechtel, F.J., Bahreini, R., Ng, N.L., Keywood, M.D., Kroll, J.H., Flagan, R.C., Seinfeld, J.H., Lee, A., Goldstein, A.H., 2006. Hygrosgopicity of secondary organic aerosols formed by oxidation of cycloalkenes, monoterpenes, sesquiterpenes, and related compounds. Atmos. Chem. Phys. 6, 2367–2388.

Wagner, R., Ajtai, T., Kandler, K., Lieke, K., Linke, C., Müller, T., Schnaiter, M., Vragel, M., 2012. Complex refractive indices of Saharan dust samples at visible and near UV wavelengths: a laboratory study. Atmos. Chem. Phys. 12, 2491–2512.

Wang, L., Li, Z.Q., Tian, Q.J., Ma, Y., Zhang, F.X., Zhang, Y., Li, D.H., Li, K.T., Li, L., 2013. Estimate of aerosol absorbing components of black carbon, brown carbon, and dust from ground-based remote sensing data of sun-sky radiometers. J. Geophys. Res. 118, 6534–6543.

WMO, 2008. Guide to Meteorological Instruments and Methods of Observation, seventh ed. (WMO No.8).

Wozniak, A.S., Shelley, R.U., Sleighter, R.L., Sleighter, R.L., Abdulla, H.A.N., Morton, P.L., Landing, W.M., Hatcher, P.G., 2013. Relationships among aerosol water soluble organic matter, iron and aluminum in European, North African, and Marine air masses from the 2010 US GEOTRACES cruise. Mar. Chem. 154, 24–33.

Xie, Y., Li, Z., Zhang, Y.X., Zhang, Y., Li, D.H., Li, K.T., Xu, H., Zhang, Y., Wang, Y.Q., Chen, X.F., Schauer, J.J., Bergin, M., 2017. Estimation of atmospheric aerosol composition from ground-based remote sensing measurements of Sun-sky radiometer. J. Geophys. Res. Atmos. http://dx.doi.org/10.1002/2016JD025839.

Xie, Y., Li, Z., Li, L., Wang, L., Li, D., Chen, C., Li, K., Xu, H., 2014. Study on influence of different mixing rules on the aerosol components retrieval from ground-based remote sensing measurements. Atmos. Res. 145–146, 267–278.

Yang, M., Howell, S.G., Zhuang, J., Huebert, B.J., 2009. Attribution of aerosol light absorption to black carbon, brown carbon, and dust in China – interpretations of atmospheric measurements during EAST-AIRE. Atmos. Chem. Phys. 9, 2035–2050. http://dx.doi.org/10.5194/acp-9-2035-2009.

Zappoli, S., Andracchio, A., Fuzzi, S., Facchini, M.C., Gelencsér, A., Kiss, G., Krivácsy, Z., Molnár, Á., Mészáros, E., Hansson, H.-C., Rosman, K., Zebühr, Y., 1999. Inorganic, organic and macromolecular components of þne aerosol in di¤erent areas of Europe in relation to their water solubility. Atmos. Environ. 33, 2733–2743.

Zhang, W.-C., Augustin, M., Zhang, Y., Li, Z., Xu, H., Liu, D., Wang, Z., Zhang, Y.-H., Ma, Y., Zhang, F., Lv, Y., 2014. Spatial and temporal variability of aerosol vertical distribution based on lidar observations: a haze case study over Jinhua Basin. Adv. Meteorol. 2014, 349592 (1-8).

Zhang, X.Q., Mcmurry, P.H., Hering, S.V., Casuccio, G.S., 1993. Mixing characteristics and water content of submicron aerosols measured in Los Angeles and at the Grand Canyon. Atmos. Environ. 27A (10), 1593–1607.

Zhang, Y., Li, Z., Zhang, Y.H., Li, D., Qie, L., Che, H., Xu, H., 2017. Estimation of aerosol complex refractive indices for both fine and coarse modes simultaneously based on AERONET remote sensing products. Atmos. Meas. Tech. 10, 3203–3213.

Zhang, Y., Li, Z., Zhang, Y.-H., Chen, Y., Cuesta, J., Ma, Y., 2016. Multi-peak accumulation and coarse modes observed from AERONET retrieved aerosol volume size distribution in Beijing. Meteorol. Atmos. Phys. http://dx.doi.org/10.1007/s00703-016-0435-3.

Zhang, Y., Li, Z., Cuesta, J., Li, D., Wei, P., Xie, Y., Li, L., 2015. Aerosol column size distribution and water uptake observed during a major haze outbreak over Beijing on January 2013. Aerosol Air Qual. Res. 15, 945–957.